

# SphOR: A Representation Learning Perspective on Open-set Recognition for Identifying Unknown Classes in Deep Learning Models.

Nadarasar Bahavan<sup>†</sup>, Sachith Seneviratne<sup>†</sup>, Saman Halgamuge<sup>†</sup>

Dept. of Mechanical Engineering  
The University of Melbourne<sup>†</sup>

bahavant@student.unimelb.edu.au, {sachith.seneviratne,saman.halgamuge}@unimelb.edu.au

## Abstract

*The widespread use of deep learning classifiers necessitates Open-set recognition (OSR), which enables the identification of input data not only from classes known during training but also from unknown classes that might be present in test data. Many existing OSR methods are computationally expensive due to the reliance on complex generative models or suffer from high training costs.*

*We investigate OSR from a representation-learning perspective, specifically through spherical embeddings. We introduce SphOR, a computationally efficient representation learning method that models the feature space as a mixture of von Mises-Fisher distributions. This approach enables the use of semantically ambiguous samples during training, to improve the detection of samples from unknown classes.*

*We further explore the relationship between OSR performance and key representation learning properties which influence how well features are structured in high-dimensional space.*

*Extensive experiments on multiple OSR benchmarks demonstrate the effectiveness of our method, producing state-of-the-art results, with improvements up-to 6% that validate its performance.*

## 1. Introduction

Traditional classification algorithms typically assume all classes associated with test data are known and already seen during training. However, in practical applications, the knowledge of classes can be incomplete, and unknown classes may be present in the test data. For example, a self-driving car trained on common road objects like cars, pedestrians, bicycles, and traffic signs may suddenly encounter an animal crossing the street or an overturned truck—objects it was never explicitly trained to classify. Traditional classifiers attempt to align these samples of unknown origin to known classes and are guaranteed to misclassify these un-

known samples into known classes, posing safety risks in critical applications like medical diagnosis or autonomous driving. Open Set Recognition (OSR) addresses this issue by allowing systems to label samples from unknown classes as ‘unknown’, while still maintaining high accuracy on known classes [37].

Deep Learning Classifiers consist of an encoder architecture for feature extraction and a neural network classifier for classification. The encoder encodes images into a compressed representation space, where features/representation/embeddings capture semantic relationships. Closer points correspond to images with similar attributes, while distant points represent images with distinct attributes. The classifier then divides this representation space, associating each region (corresponding to a set of image attributes) with a specific class. Conventional classifiers allocate the entire representation space to known classes, leaving no explicit region for unknown samples, forcing them into known categories. In contrast, OSR methods explicitly divide the space into a closed space (for known classes) and an open space (for unknown classes) [37].

Most OSR methods model representations in Euclidean space [5, 6, 47, 51], where feature magnitudes can grow arbitrarily, leading to an unbounded open space. Lubbering et al. [27] points out that an unbounded open space increases the risk of misclassifying known class samples as unknown classes, that is, open-space risk.

Since the representations encode image attributes, OSR methods are better at detecting when familiar attributes are missing rather than identifying novel attributes [10]. This implies that for effective open set detection, it is crucial to focus on learning the most distinctive attributes of each class, without shared attributes between known classes, ensuring that the classifier can accurately partition the representation space and flag images that lack these learned characteristics as unknown [10]. In this context, Liu [25] argued that optimizing intraclass compactness - ensuring that representations from the same class cluster tightly together - and interclass separability - ensuring that represen-

tations from different classes are well separated - is crucial for learning distinctive attributes via a specialized loss function.

However, an unknown sample may exhibit a blend of distinctive attributes from different known classes. In such cases, there is a risk of misclassifying it as one of the known classes. This happens because many OSR methods rely on hard labels during training, which make strict decisions about class membership. To address this, the representation space must be designed to reserve regions in the open space for samples that represent a blend of these distinctive attributes, allowing for the proper identification of unknown classes.

OSR methods are typically categorized as ‘Discriminative’ or ‘Generative’ [11]. Discriminative methods for OSR focus on learning robust classifiers with the capacity to reject samples from unknown classes [2, 5, 6, 47, 51]. However, these methods typically struggle to accurately model the open space [45]. Generative methods learn the underlying distribution of known classes using models like generative models or autoencoders [16, 19, 33, 34, 36, 39]. However, they increase the training costs of the system, are not compatible with large scale benchmarks, and face performance degradation when the unknown class samples are similar to the known class samples [16, 41, 46].

To address the limitations, we make the following contributions:

- We present a framework that learns representations with the most distinctive attributes for each class by optimizing both intra-class compactness and inter-class separability of the representations. The feature representations are modeled on spherical space, which helps constrain the open space. A detailed explanation of this approach is provided in Section 3. In Section 2.1, we demonstrate that our method has low training complexity.
- We represent each class with a prototype, which serves as the central point of the class feature distribution. The distributions are modeled using von Mises-Fisher distributions, which describe how data points are spread around their respective prototypes on the hypersphere.
- We introduce a soft class assignment mechanism during training. Unlike traditional hard assignments—where each feature is strictly associated with a single class prototype—our approach allows for a fuzzy association, where each feature can have a probabilistic connection with multiple class prototypes. To optimize this framework, we propose the Generalized von Mises-Fisher Spherical Loss, which is detailed in Section 3.1.2. This loss helps mitigate common issues in other open-set frameworks.
- Through ablation studies in Section 5, we demonstrate that high-quality feature representations, evaluated using various established quality metrics in the literature [24,

43], result in improved OSR performance.

- We show how techniques like Mixup and Label smoothing help reduce the misclassification of unknown classes that exhibit mixed distinctive features. Additionally, we introduce new metrics to evaluate different aspects of our representations and analyze the impact of these techniques. This analysis provides insights into why Mixup and label smoothing enhance OSR performance, as discussed in Section 5.
- We also highlight that our method maintains strong closed-set accuracy, as shown in Section 5.
- To our knowledge, our method achieves state-of-the-art performance on open-set recognition, outperforming prior works on benchmarks proposed by Chen, Neal, and Zhou [6, 33, 50] and detailed in Section 4.

## 2. Related Work

Open-set methods are either ‘Discriminative’ or ‘Generative’ [11]. Discriminative methods for OSR focus on learning better classifiers with the capacity to reject unknown samples. OpenMax was a popular extension to the softmax classifier, which modeled the known class features with Weibull distributions and rejected samples based on Extreme Value Theory [2]. PROSER introduced an alternative training strategy such that the rejection thresholds for each class adaptively adjust during inference [51]. These methods struggle to model the open-space [44]. Alternatively, prototype-based methods were introduced. These methods identify classes and reject unknown samples based on the distance to a class prototype. Yang et al. proposed a prototype model which models class features in Euclidean space [47]. Chen et al. extended this concept by introducing reciprocal points to represent the open-space regions in euclidean space (OSR) [5, 6]. However, euclidean space is difficult to model due to its unbounded nature.

Generative methods for OSR model the distribution or the manifold of the known classes. Some methods focus on generating difficult images while others attempt to see if it can be reconstructed from the learnt model. Neal et al. proposed a method using GANs to generate samples close to the training data but not belonging to any of the classes to train a classifier [32]. OpenGAN uses a discriminator to train the model [19]. Ozha et al. were the first to use an autoencoder and its reconstruction errors to capture open-set samples [34]. Huang et al. extended this to class-specific encoders and decoders [16]. Sun et al. extended it with VAEs [39]. Some work combine both concepts as proposed in GFROSR [36]. However, these methods increase the training costs of the system, are not compatible with large-scale benchmarks, and face performance degradation when the unknown class samples are similar to the known class samples [16, 41, 46].

More recent methods have emerged that break out of

these paradigms. Wang et al. introduced a mixture of experts for open-set detection [45]. Xu et al. proposed a method based on Supervised Contrastive Learning [46]. However, these are not scalable and will be discussed in Section 2.1.

## 2.1. Spherical Representation Learning Methods

Numerous studies have explored learning representations on hyperspheres, particularly in the context of face recognition, contrastive learning, and related fields [1, 9, 17, 26, 42].

Face recognition algorithms, such as those proposed by [9], [26], and [42], model features on the hypersphere. Additionally, metric learning methods, such as ProxyAnchor [12], have been proposed. However, these methods often face limitations, such as the strict assignment of classes and the need for fine-tuning margin hyperparameters—issues that our system effectively addresses.

Contrastive learning has gained significant traction, particularly for unsupervised data [13], while supervised contrastive learning has demonstrated notable success in supervised settings [17]. However, both approaches often rely on large batch sizes ( $B$ ) for effective learning, resulting in quadratic training complexities of  $\mathbf{O}(B^2)$ . In contrast, our method offers a substantial improvement, achieving a linear training complexity of  $\mathbf{O}(CB)$ , where  $C$  represents the class size and generally  $C < B$ . This reduction in complexity leads to significant gains in training efficiency, making our approach more scalable and resource-friendly.

## 3. Method

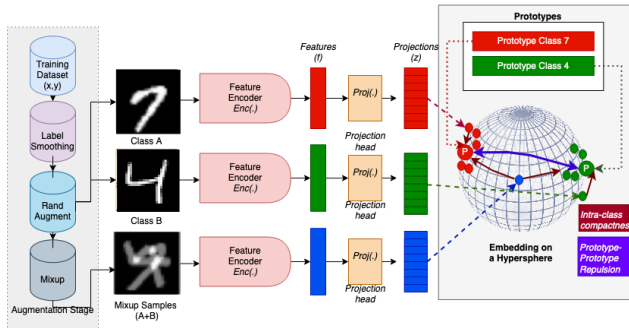


Figure 1. Our method promotes intra-class compactness and inter-class separability through a soft assignment mechanism, where samples are softly associated with their respective class prototypes based on their label information, rather than being strictly assigned. Additionally, we generate semantically vague samples using Mix-up during training. Concurrently, the method ensures that prototypes remain sufficiently distinct by repelling them from one another.

In our approach, we begin by considering a batch of la-

beled training samples  $\{\mathbf{x}_k, \mathbf{y}_k\}_{k=1}^N$ , where each  $\mathbf{x}_k$  is an image, and  $\mathbf{y}_k$  is its corresponding label selected from  $C$  classes. To enhance generalization and robustness, we generate an augmented multi-viewed batch of  $2N$  samples, denoted as  $\{\tilde{\mathbf{x}}_\ell, \tilde{\mathbf{y}}_\ell\}_{\ell=1}^{2N}$  using RandAugment [8].

During training, we apply label smoothing to the true class labels [31]. Label smoothing encourages a soft assignment of samples to class prototypes rather than a hard, one-hot encoding, thereby modeling uncertainty in the learning process. Label smoothing is applied, for each sample  $i$ , with true class label  $j$ , the smoothed label  $\tilde{y}_i = [y_{i1}, y_{i2}, \dots, y_{iC}]$  is defined as:

$$y_{ij} = 1 - \sigma, \quad y_{iq} = \frac{\sigma}{m-1} \quad \text{for } j \neq q, \quad (1)$$

where  $\sigma$  is the smoothing coefficient and  $m$  is the total number of classes.  $y_{ij}$  refers to the probability sample  $i$  belongs to class  $j$ , allowing for a soft assignment of class membership rather than a strict, discrete classification. If  $\sigma$  is 0, we get the non-smoothed labels. We will investigate the effects of label smoothing in Section 5.

Additionally, for each batch we apply Mixup [49] to create samples with ambiguous semantics:

$$x_{i,\hat{j},\alpha} = \alpha \tilde{x}_i + (1 - \alpha) \tilde{x}_j, \quad y_{i,\hat{j}} = \alpha \tilde{y}_i + (1 - \alpha) \tilde{y}_j, \quad (2)$$

where  $\alpha$  is sampled from the Beta distribution, i.e.  $\alpha \sim \text{Beta}(1, 1)$ . All these steps are the augmentation Stage in Fig 1. We will investigate the effects of Mixup in Section 5.

The augmented images  $\{\tilde{\mathbf{x}}_\ell, \tilde{\mathbf{x}}_\ell, [\tilde{\mathbf{y}}_\ell, \tilde{\mathbf{y}}_\ell]\}$  are passed through an encoder network  $Enc(\cdot)$ , producing an  $d$ -dimensional embedding:  $\mathbf{f}_i = Enc(\tilde{\mathbf{x}}_i)$ . These embeddings are further processed by a projection network, which consists of a linear layer, yielding projections  $\tilde{z}_i = Proj(\mathbf{f}_i)$ . We implement the projector network based on the work by Khosla [17],

The final embeddings are normalized as  $\mathbf{z} = \tilde{z} / \|\tilde{z}\|_2$ . We use our proposed GvMPL loss, described in Section 3.1, to train the model, shown in Fig 1, with normalized embeddings.

### 3.1. von Mises Fischer Spherical Loss (vMFSL)

The von Mises-Fisher (vMF) distribution is the hyperspherical analogue of the Gaussian distribution in Euclidean space [1, 28]. The probability density function for a unit vector  $\mathbf{z} \in \mathbb{R}^p$  in class  $c$  is given by:

$$p(\mathbf{z}; \boldsymbol{\mu}_c, \kappa) = R_p(\kappa) \exp(\kappa \boldsymbol{\mu}_c^\top \mathbf{z}), \quad (3)$$

where  $p$  is the dimensions of the projection,  $\boldsymbol{\mu}_c$  is the normalized class prototype on the unit-hyper-sphere,  $\kappa$  is the concentration factor. A higher value of  $\kappa$  results in a stronger concentration of the distribution around  $\boldsymbol{\mu}$ . In the case where  $\kappa$  approaches 0, the points become increasingly

uniformly distributed across the hyper-sphere, and  $R_p(\kappa)$  is a normalization factor [1, 28].

$\kappa$  can be interpreted as the inverse temperature parameter ( $\kappa = \frac{1}{\tau}$ ), and we fix this to a high value equally for all the classes to encourage tighter concentrations of the samples leading to intra class compactness.

Under this probability model, an projection vector  $\mathbf{z}$  is assigned to class  $c$  with the following normalized probability:

$$\mathbb{P}(y = c | \mathbf{z}; \{\boldsymbol{\mu}_j\}_{j=1}^C) = \frac{R_p(\frac{1}{\tau}) \exp(\frac{1}{\tau} \boldsymbol{\mu}_c^\top \mathbf{z})}{\sum_{j=1}^C R_p(\frac{1}{\tau}) \exp(\frac{1}{\tau} \boldsymbol{\mu}_j^\top \mathbf{z})} \quad (4)$$

$$= \frac{\exp(\boldsymbol{\mu}_c^\top \mathbf{z} / \tau)}{\sum_{j=1}^C \exp(\boldsymbol{\mu}_j^\top \mathbf{z} / \tau)}. \quad (5)$$

We set  $\tau = 0.1$  as it is the standard used in other methods[17, 46]. We perform maximum likelihood estimation on Eq. 4 with the training data to obtain:

$$\mathcal{L}_{\text{vMFSL}} = -\frac{1}{N} \sum_{i=1}^N \log \frac{\exp(z_i^\top \boldsymbol{\mu}_{c(i)} / \tau)}{\sum_{j=1}^C \exp(z_i^\top \boldsymbol{\mu}_j / \tau)}, \quad (6)$$

where  $i$  is the index of the projection,  $c(i)$  is the target class of the  $i^{\text{th}}$  sample and  $N$  is the size of the training set.

### 3.1.1. Inter-Class Separability

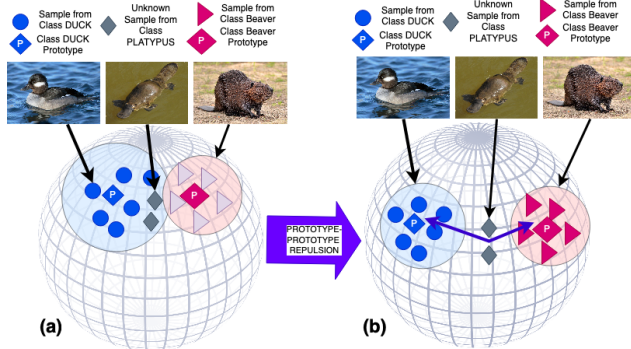


Figure 2. Illustration of the effect of optimizing only the von Mises-Fisher distribution for intra-class compactness (a), where class prototypes may become too close, leading to potential misclassification of unknown class samples. By adding an additional loss term to optimize prototype-prototype repulsion (b), we enhance inter-class separability, reducing the risk of misclassifying ambiguous unknown class samples. The effect shown is the platypus class which shares features with the beaver and duck class.

In this section, we highlight a shortcoming of optimizing only Equation 6. The current formulation ensures that each sample is assigned to its corresponding von Mises-Fisher

distribution around its class prototype, with a fixed concentration parameter  $\kappa = 1/\tau = 10$ . While this promotes intra-class compactness, it does not explicitly enforce sufficient inter-class separability. As a result, class prototypes can become close to each other, leading to the scenario illustrated in Fig. 2(a). To mitigate this issue, we add an additional loss term that explicitly optimizes prototype-prototype repulsion, leading to the scenario illustrated in Fig. 2(b).

$$\mathcal{L}_{\text{reg}} = -\frac{1}{C} \sum_{i=1}^C \frac{1}{C-1} \log \left( \sum_{\substack{j=1 \\ j \neq i}}^C \exp \left( \frac{\boldsymbol{\mu}_j^\top \boldsymbol{\mu}_i}{\tau} \right) \right). \quad (7)$$

This reduces the risk of misclassifying ambiguous unknown class samples as shown in the Fig. 2. The optimization objective would be:  $\mathcal{L}_{\text{obj}} = \mathcal{L}_{\text{vMFSL}} + \beta * \mathcal{L}_{\text{reg}}$  where  $\beta$  is a tunable hyperparameter.

### 3.1.2. Generalized von Mises Fischer Spherical Loss (GvMFSL)

We highlight a shortcoming of optimizing only  $\mathcal{L}_{\text{obj}}$ .

In the context of open-set recognition, during testing, we encounter unknown classes that exhibit a mixture of distinctive features. These unknown classes should not be mapped close to the known classes, as this could lead to misclassification.

We simulate these unknown samples via mixup, where we linearly interpolate between images to simulate samples with a mixture of distinctive features. However,  $\mathcal{L}_{\text{obj}}$  is not compatible with Mixup. Therefore, we modify it to incorporate soft labels.

Suppose we consider a sample  $(x_i, y_i)$ , then our loss is:

$$\mathcal{L}_{\text{GvMFSL}} = -\frac{1}{N} \sum_{i=1}^N \sum_{k=1}^C S_{ij} \log P_{ij} \quad (8)$$

$$\mathbb{P}(y = k | \mathbf{z}_i; \{\boldsymbol{\mu}_j\}_{j=1}^C) = P_{ik} = \frac{e^{(z_i^\top \boldsymbol{\mu}_k / \tau)}}{\sum_{j \in C} e^{(z_i^\top \boldsymbol{\mu}_j / \tau)}}. \quad (9)$$

Where  $\tilde{y}_i = [y_{i1}, y_{i2}, \dots, y_{iC}]$ , and  $S_{ik} = \frac{y_{ik}}{\sum_{j \in C} y_{ik}}$ .

**Lemma:** The first derivative of the loss for a sample  $i$  is:

$$\frac{\partial \mathcal{L}_{\text{GvMFSL}}}{\partial z_i} = \sum_{j \in C} [S_{ij} - P_{ij}] (\boldsymbol{\mu}_j / \tau) \quad (10)$$

Thus, minimizing this loss adjusts the model's parameter to align the mixed labels  $S_{ij}$  with the class membership probability  $P_{ij}$ . This loss structures the spherical representation space based on the label information. Proof is in the Supplementary Section.



Most intra-class compactness and inter-class separability methods use binary labels, enforcing discrete similarity and ignoring semantic ambiguity. However, by using our loss and mixup, we can restructure the latent space such that there are smoother transitions between the representations of known classes. This is because mixup linearly interpolates between classes, leading to a linear transition between class prototypes in the latent space. Thus, our overall training objective is:  $\mathcal{L}_{\text{obj}} = \mathcal{L}_{\text{GvMFSL}} + \beta \cdot \mathcal{L}_{\text{reg}}$  where  $\beta$  is a tunable hyperparameter.

### 3.1.3. Classifier Training and Inference

Once we learn the representations, we train a linear classifier on the frozen encoder’s representations using cross-entropy loss. The linear layer  $\phi()$  maps each feature to class probabilities through a temperature-scaled softmax function:

$$y'_i = \frac{e^{\frac{\phi(f_i(x))}{\tau}}}{\sum_{j=1}^k e^{\frac{\phi(f_j(x))}{\tau}}}, \quad (7)$$

where  $\tau$  is the temperature parameter.

For inference, we use the trained classifier and feature extractor following the methodology in Vaze and Xu et al. [41, 46]. At the end of the training phase, rejection thresholds for identifying unknown instances are established. For each training sample  $(x, y)$  belonging to class  $i$ , if  $i = \arg \max_j \phi_j(f(x))$  (indicating correct classification), the corresponding logit, i.e.  $\phi_i(f(x))$ , is stored in the class-specific logit set  $T_i$ . Once all training samples have been processed, the rejection threshold for class  $i$ , denoted as  $\epsilon_i$ , is set as the  $\lambda$ -percentile of the logit values in  $T_i$ .

During inference, a test sample  $x$  is classified as an unknown instance if  $\max_i \phi_i(f(x)) < \epsilon_i$ . The rejection thresholds can be adjusted by tuning the hyperparameter  $\lambda$ . By default, we set  $\lambda = 1\%$ , which corresponds to the target false negative rate on the training set.

## 4. Results

We evaluated our proposed method against state-of-the-art open-set recognition (OSR) approaches on standard benchmark datasets, assessing its performance on open-set recognition tasks. For a fair comparison, we pick methods that use VGG32, as the choice of backbone impacts the results or explicitly indicates cases where different backbones are used, as these variations can affect performance [32].

Our contrastive learning framework employs a linear projection network with 128 nodes, while the classification network consists of an MLP with a single fully connected layer of 128 nodes. We follow the same training protocol as ConOSR [46].

### 4.1. Unknown Detection

We follow the evaluation protocol from [32, 36, 48]. It has four datasets; each dataset is partitioned into five predefined splits, each split assigning a distinct set of  $N_{\text{train}}$  known classes. The remaining  $N_{\text{test}}$  classes in the dataset, excluding the selected known classes, serve as unknown classes for their corresponding split. To ensure robustness, we report the mean performance across these five splits.

Considering the complexity of real-world scenarios, where the ratio of seen to unseen data varies between tasks, we use openness to quantify the dataset’s complexity[46].

Openness is defined as  $1 - \sqrt{\frac{N_{\text{train}}}{N_{\text{test}}}}$ .

We use the following datasets and splits: **MNIST/CIFAR10(C10)** [20, 23]: These datasets each contain 10 classes, with CIFAR10 featuring images of vehicles and animals. We randomly select six classes as known and treat the remaining four classes as unknown. The openness for this setup is 22.54%. **CIFAR+10(C+10)** [32] and **CIFAR+50(C+50)**: To increase the openness, we choose four classes from CIFAR10 as known and sample 10 and 50 additional classes from CIFAR100 as unknown, resulting in CIFAR+10 and CIFAR+50, with openness values of 46.55% and 72.78%, respectively. **Tiny-ImageNet(TIN)** [22]: Tiny-ImageNet, a subset of ImageNet, includes 200 classes. We select 20 classes as known, and the remaining 180 classes serve as unknown, leading to an openness of 68.37%.

The Area Under the ROC Curve (AUROC) is used as the evaluation metric. AUROC is a threshold-independent measure, which can be interpreted as the probability that a positive example receives a higher detection score than a negative example[52].

The results are shown in Table 1. Our method, SPHOR, achieves strong performance in open-set recognition, ranking among the best across multiple datasets. It reaches 99.7% on MNIST, matching the highest reported results, and 94.7% on CIFAR10, slightly improving over ConOSR (94.2%) and ARPL (91.0%). On CIFAR+10 and CIFAR+50, it achieves 98.3% and 97.1%, performing competitively with ConOSR (98.1% and 97.3%). Compared to earlier approaches like Softmax, OpenMax, and C2AE, our method shows consistent improvements, particularly on more challenging datasets. These results highlight SPHOR as an effective approach for unknown class recognition.

### 4.2. Experiments for Out-of-Distribution Detection

In open-set recognition, the challenge is distinguishing known classes from unknown ones, with unknown data varying in similarity to the training distribution. However, this is a subset of the broader problem of Out-of-Distribution (OOD) detection, which aims to identify any data sample that deviates significantly from the

Table 1. Comparison of open-set recognition methods using AUROC, averaged over five trials for each dataset. Bold values indicate the best performance. N.R denotes missing results from the original paper. Benchmark from [33] and results taken from [44, 46]. Abbreviation for each venue: C-CVPR, A-AAI, T-TPAMI, E-ECCV, I-ICLR

Methods	MNIST	C10	C+10/C+50	TIN
<i>Openness%</i>	22.5	22.5	46.5 / 72.7	68.3
Softmax(I16)[14]	97.8	67.7	81.6/80.5	57.7
OpenMax(C16)[3]	98.1	69.5	81.7/79.6	57.6
OSRCI(E18)[33]	98.9	69.9	83.8/82.7	58.6
C2AE(C19)[34]	98.9	71.1	81.0/80.3	58.1
GFROSR(C20)[36]	N.R	83.1	91.5/91.3	64.7
PROSER(C21)[51]	N.R	89.1	96.0/95.3	69.3
ARPL(T21)[6]	99.7	91.0	97.1/95.1	78.2
DIAS(E2)[30]	N.R	85.0	92.0/91.6	73.1
ConOSR(A23)[46]	<b>99.7</b>	94.2	98.1/ <b>97.3</b>	80.9
MEDAF(A24)[44]	N.R	86.0	96.0/95.5	80.0
SPHOR	<b>99.7</b>	<b>94.7</b>	<b>98.3/97.1</b>	<b>81.0</b>

training distribution, regardless of its similarity to known categories[41]. Near-OOD data shares structural and visual similarities with the known classes, but with a semantic shift—it belongs to different categories, making it harder to detect. In contrast, far-OOD data represents a more significant semantic and visual shift, coming from entirely different distributions with little to no overlap with the known data. This distinction between near and far OOD is crucial for real-world applications, where novel yet related categories are often encountered.

Following the protocol in [5], we use CIFAR-10 as the in-distribution dataset and CIFAR-100 and SVHN as near-OOD and far-OOD datasets, respectively. We follow the same training backbone and methodology as previous benchmarks[6].

This benchmark utilizes the following metrics from Chen et al. [7]: **Detection accuracy (DTACC)**: This metric measures the highest classification accuracy for known and unknown samples across all possible thresholds. In the accuracy calculation, it is assumed that positive and negative samples have an equal probability of appearing in the test set **Area Under the Precision-Recall Curve (AUPR)**: Precision and recall are computed for different thresholds, and the resulting values are used to generate the curve. AUPR is then calculated as the area under this curve. Additionally, AUPR is computed separately for two cases: one where in-distribution samples are considered positive (resulting in AUIN), and one where out-of-distribution samples are considered positive (resulting in AUOUT). **TNR** is  $\frac{TN}{TP+TN}$ , when  $TPR = \frac{TP}{FP+FN} = 0.95$ .

As shown in Table 2, SPHOR outperforms all SOTA

methods in nearOOD detection with an AUROC of 93.7, significantly surpassing previous methods. In farOOD detection, SPHOR achieves a competitive AUROC of 99.3, comparable to the best-performing methods. This demonstrates that SPHOR excels in distinguishing nearOOD data, while maintaining strong performance for farOOD detection.

### 4.3. Experiments for Open-Set Detection

This open-set recognition benchmark tests a model’s ability to classify known classes while detecting unseen ones. We follow Zhou et al. [51]’s protocol using MNIST and CIFAR-10. In testing, samples from a different dataset are added as unknown classes. Performance is measured with macro-averaged F1 scores, covering both known and open-set classes. The **macro-averaged F1 score** is the average of the F1 scores computed for each class individually, treating all classes equally regardless of their frequency [6].

Our first experiment trains on MNIST and tests on three datasets: Omniglot (OmniG) [21], MNIST-Noise (NMNIST), and Noise (NOISE). Following [51], we include 10,000 unknown samples to match the number of known test samples. Since Omniglot’s test set has 13,180 images, we use the first 10,000 sorted by filename index. The Noise dataset is generated by sampling each pixel from a uniform distribution [0,1], while MNIST-Noise is created by over-laying these noise images onto MNIST test samples.

In the second experiment, we train on CIFAR-10 and use TinyImageNet and LSUN as unknown test samples. Each dataset has 10,000 test images. To account for size differences, we process the unknown images in two ways: (1) resizing them to 32×32 (LR, TIR) and (2) cropping a 32×32 patch from each image (LC, TIC).

Our results demonstrate strong performance across multiple benchmarks. As shown in Table 3,4, SPHOR effectively handles open-set classes from diverse inputs and outperforms state-of-the-art methods.

## 5. Analysis

To assess the quality of the learned representations, we use the concepts of Uniformity and Alignment for supervised learning on the hyper-sphere [24, 43].

One of the objectives of our loss function is to minimize the distance between features of the same class, ensuring intra-class compactness. Thus, Alignment is defined as the average pairwise distance between samples of the same class. Given that  $F_i$  represents the set of normalized features for class  $i$ , Alignment is defined as:  $A = \frac{1}{C} \sum_{i=1}^C \frac{1}{|F_i|^2} \sum_{v_j, v_k \in F_i} \|f_j - f_k\|^2$ . [24]

Another objective is to ensure that classes are as spread out as possible on the hypersphere, promoting inter-class separability. Uniformity is defined as the average pairwise

Table 2. Distinguishing In-Distribution and Out-of-Distribution Data for Image Classification Across Different Validation Setups (Benchmark from [6]) Results taken from [44]. Results shown using VGG32 backbone.

Method	In:CIFAR10 / Out:CIFAR100					In:CIFAR10 / Out:SVHN				
	TNR	DTACC	AUROC	AUIN	AUOUT	TNR	DTACC	AUROC	AUIN	AUOUT
SoftMax (ICLR'16)[14]	31.9	79.8	86.3	88.4	82.5	32.1	86.4	90.6	88.3	93.6
GCPL (TPAMI'20)[47]	35.7	80.2	86.4	86.6	84.1	41.4	86.1	91.3	86.6	94.8
RPL (ECCV'20)[4]	32.6	80.6	87.1	88.8	83.8	41.9	87.1	92.0	89.6	95.1
ARPL (TPAMI'21)[6]	48.5	83.4	90.3	91.1	88.4	79.1	91.6	96.6	94.8	98.0
CSI (NeuroIPS'20)[40]	NR	84.4	91.6	92.5	90.0	NR	92.8	97.9	96.2	99.0
OpenGAN (ICCV'21)[18]	NR	84.2	89.7	87.7	89.6	NR	92.1	95.9	93.4	97.1
CSSR (TPAMI'22)[15]	NR	83.8	92.1	89.4	89.3	NR	95.7	99.1	98.2	<b>99.6</b>
RCSSR (TPAMI'22)[15]	NR	85.3	92.3	92.9	91.0	NR	95.7	99.1	98.3	<b>99.6</b>
MEDAF (AAAI'24)[44]	NR	85.4	92.5	93.2	91.1	NR	95.3	99.1	98.0	<b>99.6</b>
SPHOR	<b>64.49</b>	<b>87.4</b>	<b>93.7</b>	<b>94.4</b>	<b>92.4</b>	<b>98.1</b>	<b>96.6</b>	<b>99.3</b>	<b>99.4</b>	98.6

Table 3. Open-set recognition results on MNIST are presented with unknown datasets added to the test set as unknown classes (Benchmark from [50]). Performance is evaluated using macro F1 across 11 classes (10 known and 1 unknown). A false negative rate  $\lambda = 1\%$ ,  $\lambda = 2\%$  are considered when selecting the classifier rejection threshold. Results shown using VGG32 backbone.

Methods	OmniG	NMNIST	NOISE
Softmax(ICLR'16)	59.5	64.1	82.9
OpenMax(CVPR'16) [3]	68.0	64.1	82.6
CROSR(CVPR'20) [33]	79.3	72.0	82.6
PROSER(CVPR'21) [48]	86.2	82.7	88.2
ConOSR(AAAI'23) [36]	95.4	98.7	98.8
SPHOR ( $\lambda = 1\%$ )	<b>95.5</b>	<b>98.8</b>	<b>98.9</b>
SPHOR ( $\lambda = 2\%$ )	<b>96.0</b>	98.4	98.4

distance between class centroids. To measure this, Uniformity is defined as [24]:

$$U = \frac{1}{C(C-1)} \sum_{i=1}^C \sum_{\substack{j=1 \\ j \neq i}}^C \left\| \frac{c_i}{\|c_i\|_2} - \frac{c_j}{\|c_j\|_2} \right\|^2. \quad (11)$$

where  $c_i$  and  $c_j$  are the normalized centroids of class  $i$  and class  $j$ , respectively, and  $C$  is the total number of classes. The centroid  $c_i$  is computed as the mean of the normalized feature vectors of the samples in class  $i$ :  $c_i = \frac{1}{|F_i|} \sum_{f_k \in F_i} f_k$ , where  $F_i$  represents the set of normalized feature vectors for class  $i$ , and  $|F_i|$  is the number of samples in class  $i$ .

Our classifier is trained on unnormalized features and makes decisions based on raw classifier outputs (logits) to determine whether a sample is known or unknown, following the methodology described in 3.1.3. We evaluated its performance using the AUROC metric. The  $L_2$  norm of

Table 4. Open-set recognition results on CIFAR10 are presented with unknown datasets added to the test set as unknown classes (Benchmark from [50]). Performance is evaluated using macro F1 across 11 classes (10 known and 1 unknown). A false negative rate  $\lambda = 1\%$ ,  $\lambda = 2\%$  are considered when selecting the classifier rejection threshold. Results shown using VGG32 backbone.

Methods	TIC	TIR	LC	LR
Softmax (ICLR'16)	63.9	65.3	64.2	64.7
OpenMax (CVPR'16) [3]	66.0	68.4	65.7	66.8
OSRCI (ECCV'18 [33])	63.6	63.5	65.0	64.8
CROSR (CVPR'20) [48]	72.1	73.5	72.0	74.9
GFROSR (CVPR'20) [36]	75.7	79.2	75.1	80.5
PROSER (CVPR'21) [36]	75.7	79.2	75.1	80.5
ConOSR (AAAI'23) [36]	89.1	84.3	91.2	88.1
SPHOR ( $\lambda = 1\%$ )	<b>89.9</b>	83.3	<b>92.9</b>	<b>93.6</b>
SPHOR ( $\lambda = 2\%$ )	<b>90.6</b>	<b>84.8</b>	<b>92.7</b>	<b>93.1</b>

a feature vector,  $\|f_i\|_2 = \sqrt{\sum_{i=1}^d f_{ij}^2}$ , has been shown to correlate with confidence levels in the embeddings produced by feature encoders [35, 38]. Specifically, a higher norm indicates greater confidence in the representation, while a lower norm suggests lower confidence. Park et al. further demonstrated that *this property can be directly leveraged for Out-of-Distribution (OOD)/Outlier detection.* [35]

To capture how well the feature norms differentiate between known and unknown classes, we introduce a metric called the Norm Discriminability Index  $N_{auroc}$ . This metric measures how much the norms of the features for known and unknown classes differ. A larger difference in norms indicates a clearer separation between the known/unknown classes, while a smaller difference suggests that the model has difficulty distinguishing between them based on their

Table 5. Ablation study on the loss term with CIFAR10 (6 known classes 4 unknown) and TinyImagenet (20 known, 80 unknown) compared using various metrics such as Uniformity, alignment, OSR performance ( $A^{\text{uroc}}$ ), Semantic Discriminability Index ( $S_{\text{auroc}}$ ), Norm Discriminability Index ( $N_{\text{auroc}}$ ). For each dataset, the average metric over 5 class splits is reported to ensure the result is robust.

LS	Mixup	$\mathcal{L}_{\text{reg}}$	CIFAR10					TinyImageNet				
			$A \downarrow$	$U \uparrow$	$A^{\text{uroc}} \uparrow$	$S_{\text{auroc}} \uparrow$	$N_{\text{auroc}} \uparrow$	$A \downarrow$	$U \uparrow$	$A^{\text{uroc}} \uparrow$	$S_{\text{auroc}} \uparrow$	$N_{\text{auroc}} \uparrow$
✓	✓	✓	<b>0.47</b>	<b>4.9</b>	<b>94.5</b>	<b>92.9</b>	<b>93.0</b>	<b>0.73</b>	<b>2.27</b>	<b>81.0</b>	<b>80.5</b>	<b>77.4</b>
✓	✓	×	0.48	4.74	94.5	93.0	93.2	0.76	2.25	80.9	80.5	76.9
×	×	×	0.52	4.12	94.2	90.0	93.0	0.78	2.00	79.0	78.8	71.4
×	×	✓	0.52	4.09	94.0	90.2	89.6	0.79	1.99	79.2	79.1	70.8
✓	×	✓	0.47	4.42	93.7	92.0	90.3	0.79	2.36	79.0	78.4	76.7
×	✓	✓	0.48	4.60	94.4	93.0	93.0	0.71	1.74	79.8	79.7	70.2

norms.

We are also interested in understanding the classifier’s performance when using normalized features, thereby removing norm information. To explore this, we calculate the AUROC using a classifier trained and tested on these normalized features. Since the normalized features capture only the angular relationships between them, which encode semantic information, we refer to this metric as the Semantic Discriminability Index ( $S_{\text{auroc}}$ ) [29].

Using these metrics, we gain a deeper understanding of our framework. To interpret the effects, we adopt the methodology of Neal et al. and evaluate our approach across five different class splits on CIFAR-10 and TinyImageNet [33].

The ablation study is presented in Table 5. *We observe that AUROC is a superior metric for OSR performance.* Based on that,  $S_{\text{AUROC}}$  and AUROC are strongly influenced by alignment and uniformity. *As both alignment and uniformity improve, AUROC/ $S_{\text{AUROC}}$  steadily increases. This indicates that tightly clustered and well-separated feature spaces contribute to an enhanced Semantic Discriminability Index between known and unknown samples.* Mixup plays a crucial role in  $S_{\text{AUROC}}$ . When Mixup is applied,  $S_{\text{AUROC}}$  improves from 79.1 to 79.7 on TinyImageNet and from 90.2 to 93 on CIFAR-10. *This validates the hypothesis that due to Mixup’s smoother transitions between classes, it facilitates the detection of unknown samples with with mixed distinctive features. Label Smoothing improves  $N_{\text{AUROC}}$ :* Applying label smoothing (LS) increases  $N_{\text{auroc}}$  from 89.6 to 90.3 on CIFAR-10 and from 70.8 to 76.7 on TinyImageNet, indicating improved confidence estimates for both known and unknown samples.

*In our ablation study, we see a small improvement from using  $\mathcal{L}_{\text{reg}}$  across multiple cases.* The main improvement is via Mixup and LS. *The synergy of Mixup and LS leads to optimal OSR performance.* While each technique alone falls short of the best results, their combination improves both semantic and uncertainty separability. This indicates

that Mixup enhances latent structure, while label smoothing regulates feature confidence, making their joint application crucial for robust open-set representation learning. These findings highlight that balancing mixup and label smoothing not only strengthens feature alignment and uniformity but also improves classification and uncertainty estimation. Detailed visual analysis in the Supplementary.

**Competitive Closed Set Performance** Competitive closed-set performance is essential for robust OSR. As shown in Table 6, our results remain competitive. Comparisons on CIFAR-10 highlight that many OSR methods degrade closed-set accuracy, unlike our approach, which maintains performance. A baseline using the same data augmentation strategy is included for fairness, with networks trained on CIFAR-10/100. ARPL and MEDAF utilize stronger ResNet backbones compared to our implementation.

Table 6. Closed performance comparison in terms of accuracy on CIFAR10 and first 100 classes of TinyImageNet. SPHOR is competitive with other cutting edge OSR methods on closed set accuracy. MoE-Mixture of Experts.

Methods	CIFAR10	TIN-100
Softmax (VGG32)	94.0	63.7
ARPL (ResNet34)	94.0	65.7
ConOSR (VGG32)	94.6	66.1
MEDAF (ResNet18+MoE)	<b>95.4</b>	<b>70.6</b>
SPHOR (VGG32)	<b>95.4</b>	63.7

## 6. Limitations and Conclusions

Our method optimizes intra-class compactness and inter-class separability by representing features in spherical space using a mixture of von Mises–Fisher distributions with probabilistic class prototype associations. By integrating techniques like Mixup, we effectively reduce misclassification of unknown classes while achieving state-of-the-art



OSR performance. Ablation studies and novel evaluation metrics further demonstrate that our approach significantly enhances feature representation quality and overall OSR robustness. However, it is not without limitations. The approach currently models each class with a single prototype having fixed concentration parameters. Future work should aim to address these constraints by allowing multiple prototypes per class with dynamic concentration parameters.

## 7. Acknowledgement

NB acknowledges Melbourne Graduate Research Scholarship. We would like to thank Chathura Jayasankha, Jayanie Bogahawatte, Yu Xia and Nisal Ranasinghe for providing valuable feedback. This research was supported by The University of Melbourne’s Research Computing Services .

## References

- [1] Haoyue Bai, Yifei Ming, Julian Katz-Samuels, and Yixuan Li. Hypo: Hyperspherical out-of-distribution generalization. In *The Twelfth International Conference on Learning Representations*, Vienna, Austria, 2024. OpenReview.net. 3, 4
- [2] Abhijit Bendale and Terrance Boulton. Towards open world recognition. In *Proceedings of the IEEE/CVF Conference on Computer Vision and Pattern Recognition*, pages 1893–1902, 2015. 2
- [3] Abhijit Bendale and Terrance E. Boulton. Towards open set deep networks. In *Proceedings of the IEEE/CVF Conference on Computer Vision and Pattern Recognition*, pages 1563–1572, 2016. 6, 7
- [4] Guangyao Chen, Limeng Qiao, Yemin Shi, Peixi Peng, Jia Li, Tao Huang, Shiliang Pu, and Yonghong Tian. Learning open set network with discriminative reciprocal points. In *Computer Vision – ECCV 2020*, pages 507–522. Springer, 2020. 7
- [5] Guangyao Chen, Limeng Qiao, Yemin Shi, Peixi Peng, Jia Li, Tiejun Huang, Shiliang Pu, and Yonghong Tian. Learning open set network with discriminative reciprocal points. In *Proceedings of the European Conference on Computer Vision*, pages 507–522, 2020. 1, 2, 6
- [6] Guangyao Chen, Pai Peng, Xingyu Wang, and Yonghong Tian. Adversarial reciprocal points learning for open set recognition. *IEEE Transactions on Pattern Analysis and Machine Intelligence*, pages 1–1, 2021. 1, 2, 6, 7
- [7] Guangyao Chen, Peixi Peng, Xiangqian Wang, and Yonghong Tian. Adversarial reciprocal points learning for open set recognition. *IEEE Transactions on Pattern Analysis and Machine Intelligence*, 44(11):8065–8081, 2022. 6
- [8] Ekin D Cubuk, Barret Zoph, Jonathon Shlens, and Quoc V Le. Randaugment: Practical automated data augmentation with a reduced search space. In *Proceedings of the IEEE/CVF Conference on Computer Vision and Pattern Recognition Workshops*, pages 702–703, 2020. 3
- [9] Jiankang Deng, Jia Guo, Niannan Xue, and Stefanos Zafeiriou. Arcface: Additive angular margin loss for deep face recognition. In *Proceedings of the IEEE/CVF Conference on Computer Vision and Pattern Recognition (CVPR)*, 2019. 3
- [10] Thomas G. Dietterich and Alexander Guyer. The familiarity hypothesis: Explaining the behavior of deep open set methods. *Pattern Recognition*, 132:108931, 2022. 1
- [11] Chuanxing Geng, Sheng-jun Huang, and Songcan Chen. Recent advances in open set recognition: A survey. *IEEE Transactions on Pattern Analysis and Machine Intelligence*, 2020. 2
- [12] Moritz Grapow, Lukas Hübner, Ognjen Arandjelovic, and Stefan Roth. Proxyanchor: Efficient contrastive learning with proxy labels. In *Proceedings of the IEEE/CVF International Conference on Computer Vision (ICCV)*, pages 9313–9322, 2021. 3
- [13] Kaiming He, Haoqi Fan, Yuxin Wu, Saining Xie, and Ross Girshick. Momentum contrast for unsupervised visual representation learning. In *Proceedings of the IEEE/CVF Conference on Computer Vision and Pattern Recognition*, pages 9729–9738, 2020. 3
- [14] Dan Hendrycks and Kevin Gimpel. A baseline for detecting misclassified and out-of-distribution examples in neural networks. In *Proceedings of the International Conference on Learning Representations*, pages 1–12, 2016. 6, 7
- [15] Hongzhi Huang, Yu Wang, Qinghua Hu, and Ming-Ming Cheng. Class-specific semantic reconstruction for open set recognition. *IEEE Transactions on Pattern Analysis and Machine Intelligence*, 2022. 7
- [16] Hongzhi Huang, Yu Wang, Qinghua Hu, and Ming-Ming Cheng. Class-specific semantic reconstruction for open set recognition. *IEEE Transactions on Pattern Analysis and Machine Intelligence*, 45(4):4214–4228, 2023. 2
- [17] Prannay Khosla, Piotr Teterwak, Chen Wang, Aaron Sarna, Yonglong Tian, Phillip Isola, Aaron Maschiot, Ce Liu, and Dilip Krishnan. Supervised contrastive learning. *arXiv preprint arXiv:2004.11362*, 2020. 3, 4
- [18] Shu Kong and Deva Ramanan. Opengan: Open-set recognition via open data generation. In *Proceedings of the IEEE/CVF International Conference on Computer Vision (ICCV)*, pages 813–822, 2021. 7
- [19] Shu Kong and Deva Ramanan. Opengan: Open-set recognition via open data generation. *IEEE Transactions on Pattern Analysis and Machine Intelligence*, pages 1–10, 2022. 2
- [20] Alex Krizhevsky, Geoffrey Hinton, et al. Learning multiple layers of features from tiny images. Technical report, University of Toronto, 2009. 5
- [21] Brenden M. Lake, Ruslan Salakhutdinov, and Joshua B. Tenenbaum. Human-level concept learning through probabilistic program induction. *Science*, 350(6266):1332–1338, 2015. 6
- [22] Ya Le and Xuan Yang. Tiny imagenet visual recognition challenge. <https://tiny-imagenet.herokuapp.com/>, 2015. 5
- [23] Yann LeCun, Corinna Cortes, and CJ Burges. Mnist handwritten digit database. *ATT Labs [Online]*. Available: <http://yann.lecun.com/exdb/mnist>, 2, 2010. 5

- [24] Tianhong Li, Peng Cao, Yuan Yuan, Lijie Fan, Yuzhe Yang, Rogerio Feris, Piotr Indyk, and Dina Katabi. Targeted supervised contrastive learning for long-tailed recognition. In *Proceedings of the IEEE/CVF Conference on Computer Vision and Pattern Recognition*, pages 6908–6918, 2022. 2, 6, 7
- [25] Weiyang Liu, Yandong Wen, Zhiding Yu, and Meng Yang. Large-margin softmax loss for convolutional neural networks. In *Proceedings of The 33rd International Conference on Machine Learning*, pages 507–516. PMLR, 2016. 1
- [26] Weiyang Liu, Yandong Wen, Zhiding Yu, Ming Li, Bhiksha Raj, and Le Song. Sphreface: Deep hypersphere embedding for face recognition. In *2017 IEEE Conference on Computer Vision and Pattern Recognition (CVPR)*, pages 6738–6746, 2017. 3
- [27] M. Lübbering, M. Gebauer, R. Ramamurthy, et al. Bounding open space risk with decoupling autoencoders in open set recognition. *International Journal of Data Science and Analytics*, 14:351–373, 2022. 1
- [28] Kanti V. Mardia and Peter E. Jupp. *Directional Statistics*. John Wiley & Sons Ltd, 1999. 3, 4
- [29] Tomas Mikolov, Ilya Sutskever, Kai Chen, Greg S Corrado, and Jeff Dean. Distributed representations of words and phrases and their compositionality. In *Advances in Neural Information Processing Systems*, pages 3111–3119, 2013. 8
- [30] W. Moon, J. Park, H. S. Seong, C.-H. Cho, and J.-P. Heo. Difficulty-aware simulator for open set recognition. In *Proceedings of the European Conference on Computer Vision (ECCV)*, pages 365–381, 2022. 6
- [31] Rafael Müller, Simon Kornblith, and Geoffrey E Hinton. When does label smoothing help? In *Advances in Neural Information Processing Systems*, 2019. 3
- [32] Lawrence Neal, Matthew Olson, Xiaoli Fern, Weng-Keen Wong, and Fuxin Li. Open set learning with counterfactual images. In *Proceedings of the European Conference on Computer Vision (ECCV)*, pages 613–628, 2018. 2, 5
- [33] Lawrence Neal, Matthew L. Olson, Xiaoli Z. Fern, Weng-Keen Wong, and Fuxin Li. Open set learning with counterfactual images. In *Proceedings of the European Conference on Computer Vision*, pages 620–635, 2018. 2, 6, 7, 8
- [34] Poojan Oza and Vishal M. Patel. C2ae: Class conditioned auto-encoder for open-set recognition. In *Proceedings of the IEEE/CVF Conference on Computer Vision and Pattern Recognition*, pages 2302–2311, 2019. 2, 6
- [35] Jaewoo Park, Jacky Chen Long Chai, Jaeho Yoon, and Andrew Beng Jin Teoh. Understanding the feature norm for out-of-distribution detection. In *Proceedings of the IEEE/CVF International Conference on Computer Vision*, pages 1557–1567, 2023. 7
- [36] Pramuditha Perera, Vlad I. Morariu, Rameswar Jain, Varun Manjunatha, Curtis Wigington, Vicente Ordonez, and Vishal M. Patel. Generative-discriminative feature representations for open-set recognition. In *Proceedings of the IEEE/CVF Conference on Computer Vision and Pattern Recognition (CVPR)*, pages 11814–11823, 2020. 2, 5, 6, 7
- [37] Walter J. Scheirer, Anderson Rocha, Archana Sapkota, and Terrance E. Boult. Towards open set recognition. *IEEE Transactions on Pattern Analysis and Machine Intelligence*, X(X):1–1, 2012. 1
- [38] Tyler R. Scott, Andrew C. Gallagher, and Michael C. Mozer. von mises–fisher loss: An exploration of embedding geometries for supervised learning. In *Proceedings of the IEEE/CVF International Conference on Computer Vision (ICCV)*, pages 10612–10622, 2021. 7
- [39] Xin Sun, Zhenning Yang, Chi Zhang, Keck-Voon Ling, and Guohao Peng. Conditional gaussian distribution learning for open set recognition. In *Proceedings of the IEEE/CVF Conference on Computer Vision and Pattern Recognition*, pages 13477–13486, 2020. 2
- [40] Jihoon Tack, Sangwoo Mo, Jongheon Jeong, and Jinwoo Shin. Csi: Novelty detection via contrastive learning on distributionally shifted instances. In *Proceedings of the Conference on Neural Information Processing Systems*, pages 11839–11852, 2020. 7
- [41] Sagar Vaze, Kai Han, Andrea Vedaldi, and Andrew Zisserman. Open-set recognition: A good closed-set classifier is all you need. In *Proceedings of the International Conference on Learning Representations*, pages 1–14, 2022. 2, 5, 6
- [42] Hao Wang, Yitong Wang, Zheng Zhou, Xing Ji, Dihong Gong, Jingchao Zhou, Zhifeng Li, and Wei Liu. Cosface: Large margin cosine loss for deep face recognition. In *Proceedings of the IEEE Conference on Computer Vision and Pattern Recognition (CVPR)*, pages 5265–5274, 2018. 3
- [43] Tongzhou Wang and Phillip Isola. Understanding contrastive representation learning through alignment and uniformity on the hypersphere. In *International Conference on Machine Learning*, pages 9929–9939. PMLR, 2020. 2, 6
- [44] Yu Wang, Junxian Mu, Pengfei Zhu, and Qinghua Hu. Exploring diverse representations for open set recognition. In *AAAI Conference on Artificial Intelligence*, 2024. 2, 6, 7
- [45] Yu Wang, Junxian Mu, Pengfei Zhu, and Qinghua Hu. Exploring diverse representations for open set recognition. In *Proceedings of the AAAI Conference on Artificial Intelligence*, pages 5731–5739, 2024. 2, 3
- [46] Baile Xu, Furao Shen, and Jian Zhao. Contrastive open set recognition. In *Proceedings of the AAAI Conference on Artificial Intelligence*, pages 10546–10556, 2023. 2, 3, 4, 5, 6
- [47] Hong-Ming Yang, Xiao-Yan Zhang, Fei Yin, Qing Yang, and Cheng-Lin Liu. Convolutional prototype network for open set recognition. *IEEE Transactions on Pattern Analysis and Machine Intelligence*, 44(4):2358–2370, 2020. 1, 2, 7
- [48] Ryota Yoshihashi, Wen Shao, Rei Kawakami, Shaodi You, Makoto Iida, and Takeshi Naemura. Classification-reconstruction learning for open-set recognition. In *Proceedings of the IEEE/CVF Conference on Computer Vision and Pattern Recognition*, pages 4016–4025, 2019. 5, 7
- [49] Hongyi Zhang, Moustapha Cisse, Yann N. Dauphin, and David Lopez-Paz. mixup: Beyond empirical risk minimization. In *International Conference on Learning Representations*, 2018. 3
- [50] Bolei Zhou, Aditya Khosla, Agata Lapedriza, Aude Oliva, and Antonio Torralba. Learning deep features for discriminative localization. In *Proceedings of the IEEE/CVF Con-*

*ference on Computer Vision and Pattern Recognition*, pages 2921–2929, 2016. [2](#), [7](#)

- [51] Da-Wei Zhou, Han-Jia Ye, and De chuan Zhan. Learning placeholders for open-set recognition. In *2021 IEEE/CVF Conference on Computer Vision and Pattern Recognition (CVPR)*, pages 4399–4408, 2021. [1](#), [2](#), [6](#)
- [52] Kelly H. Zou, Aiyi Liu, Andriy I. Bandos, Lucila Ohno-Machado, and Howard E. Rockette. *Statistical Evaluation of Diagnostic Performance: Topics in ROC Analysis*. Chapman and Hall/CRC, 2011. [5](#)

## 8. Extended Methods

### 8.1. GvMFSL Loss Function: Proof of Lemma 01

We define the **Generalized von Mises-Fisher Supervised Loss (GvMFSL)** as:

$$\mathcal{L}_{\text{GvMFSL}} = -\frac{1}{N} \sum_{i=1}^N \sum_{k=1}^C S_{ik} \log P_{ik} \quad (12)$$

where the probability of class  $k$  given feature  $\mathbf{z}_i$  is modeled as:

$$\mathbb{P}(y = k \mid \mathbf{z}_i; \{\boldsymbol{\mu}_j\}_{j=1}^C) = P_{ik} = \frac{\exp(z_i^\top \boldsymbol{\mu}_k / \tau)}{\sum_{j \in C} \exp(z_i^\top \boldsymbol{\mu}_j / \tau)}. \quad (13)$$

Here,  $\tilde{y}_i = [y_{i1}, y_{i2}, \dots, y_{iC}]$ , and the normalized similarity score is given by:

$$S_{ik} = \frac{y_{ik}}{\sum_{j \in C} y_{ij}}. \quad (14)$$

We can rewrite the loss function as:

$$\mathcal{L}_{\text{GvMFSL}} = -\frac{1}{N} \sum_{i=1}^N L_i \quad (15)$$

where the individual loss term for sample  $i$  is:

$$L_i = \sum_{j \in C} S_{ij} \log P_{ij}. \quad (16)$$

The first derivative of the loss function with respect to feature  $z_i$  is:

$$\frac{\partial L_i}{\partial x_i} = \sum_{j \in C} S_{ij} \frac{\boldsymbol{\mu}_j}{\tau} - \sum_{j \in C} S_{ij} \sum_{k \in C} P_{ik} \frac{\boldsymbol{\mu}_k}{\tau}. \quad (17)$$

Rearranging the summations,

$$\frac{\partial L_i}{\partial x_i} = \sum_{j \in C} S_{ij} \frac{\boldsymbol{\mu}_j}{\tau} - \sum_{k \in C} P_{ik} \frac{\boldsymbol{\mu}_k}{\tau} \sum_{j \in C} S_{ij}. \quad (18)$$

Since  $\sum_{j \in C} S_{ij} = 1$ , this simplifies to:

$$\frac{\partial L_i}{\partial x_i} = \sum_{j \in C} [S_{ij} - P_{ij}] \frac{\boldsymbol{\mu}_j}{\tau}. \quad (19)$$

## 9. Extended Results

### 9.1. Openset Benchmark Breakdown

This open-set recognition benchmark tests a model's ability to classify known classes while detecting unseen ones. We follow Zhou et al. [51]'s protocol using MNIST and

CIFAR-10. In testing, samples from a different dataset are added as unknown classes. Performance is measured with macro-averaged F1 scores, covering both known and open-set classes. The **macro-averaged F1 score** is the average of the F1 scores computed for each class individually, treating all classes equally regardless of their frequency [6].

FNR( $\lambda\%$ )	TINR	TINC	LSUNR	LSUNC
1	0.833	0.899	0.936	0.929
2	0.848	0.906	0.931	0.927
3	0.855	0.908	0.925	0.922
4	0.857	0.905	0.919	0.916
5	0.858	0.902	0.914	0.911
6	0.858	0.899	0.908	0.906
7	0.856	0.895	0.903	0.902
8	0.855	0.891	0.898	0.896
9	0.853	0.886	0.892	0.891
10	0.850	0.882	0.887	0.886
11	0.847	0.877	0.882	0.881
12	0.843	0.872	0.875	0.874
13	0.839	0.866	0.870	0.869
14	0.835	0.860	0.864	0.864
15	0.830	0.855	0.858	0.857

Table 7. Values for FNR( $\lambda$ ), TINR, TINC, LSUNR, and LSUNC.

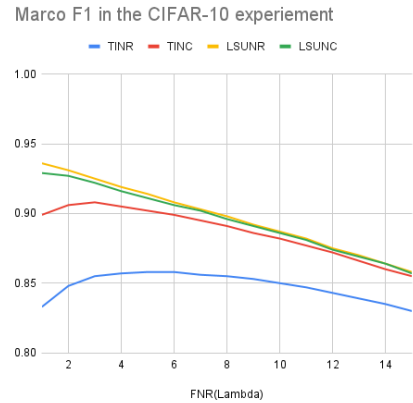


Figure 3. Macro F1 in the CIFAR-10 experiment for various rejection thresholds  $\lambda$ .



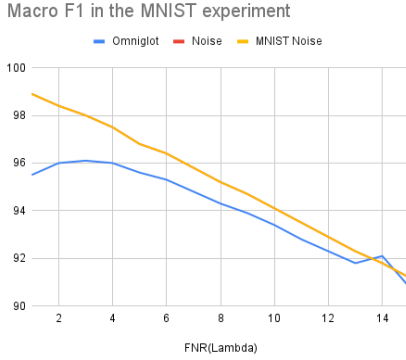


Figure 4. Macro F1 in the MNIST experiment for various rejection thresholds  $\lambda$ .

FNR( $\lambda$ )	Omniglot	Noise	MNIST Noise
1	<b>95.5</b>	<b>98.9</b>	<b>98.9</b>
2	<b>96.0</b>	<b>98.4</b>	<b>98.4</b>
3	96.1	98.0	98.0
4	96.0	97.5	97.5
5	95.6	96.8	96.8
6	95.3	96.4	96.4
7	94.8	95.8	95.8
8	94.3	95.2	95.2
9	93.9	94.7	94.7
10	93.4	94.1	94.1
11	92.8	93.5	93.5
12	92.3	92.9	92.9
13	91.8	92.3	92.3
14	92.1	91.8	91.8
15	90.8	91.2	91.2

Table 8. Values for FNR( $\lambda$ ), Omniglot, Noise, and MNIST Noise.

## 9.2. Training

### 9.2.1. Encoder

We use SGD with a learning rate of 0.05 to 0.5, a weight decay of  $1e-4$ , and a momentum of 0.9. We use a batch size of 128. To enhance stability, Adam is used for optimizing the prototypes. The temperature is set to 0.1, following the standard practice. Training hyperparameters follows the setup outlined in Xu et al.[41, 46].

### 9.2.2. Classifier

We use SGD with a learning rate of 0.02, a weight decay of  $1e-4$ , and a momentum of 0.9. We use a batch size of 128. The temperature is set to 2, following the standard practice. Training hyperparameters follows the setup outlined in Xu et al.[41, 46].

**Backbone:** The VGG32 backbone is commonly employed in open-set detection[33]. It consists of a se-

quence of nine  $3 \times 3$  convolutional layers, with downsampling achieved through strided convolutions every third layer. Batch normalization is applied after each convolutional layer. After the ninth convolutional layer, average pooling is used to reduce the spatial features to a 128-dimensional feature vector, which is then passed through a fully connected linear classifier to produce the output logits.

## 10. Extended Analysis

We continue our analysis of Mixup, label smoothing (LS), and regularization in this section using a different benchmark. Specifically, we extend our ablation studies to the NearOOD/FarOOD benchmark [6]. By replicating these experiments, we observe that the results remain consistent with our previous findings on the CIFAR10-TinyImageNet benchmark.

Table 9. Ablation study on the loss term with CIFAR10 (10 known classes) and CIFAR100 (100 unknown) compared over various metrics such as  $S_{auroc}$ ,  $N_{auroc}$ ,  $AUROC_{f(x)}$

LS	Mixup	$N_{auroc}$		$S_{auroc}$	
		C100	SVHN	C100	SVHN
✓	✓	93.3	99.3	90.0	99.2
✓	×	91.7	99.8	89.5	97.0
×	✓	90.4	99.9	91.3	98.3
×	×	87.1	99.8	91.0	92.0

### 10.0.1. TSNE Analysis

Furthermore, we visualize the feature distributions using t-SNE and investigate the links described beforehand.

**SVHN is used as the unknown dataset, while CIFAR-10 serves as the known dataset:** As observed, the classes are well-separated due to the lack of semantic similarity between them. This distinct separation makes unknown detection relatively straightforward, as illustrated in Fig. 5 and Fig. 6.

**CIFAR-100 is used as the unknown dataset, while CIFAR-10 serves as the known dataset:** Unlike SVHN, CIFAR-100 contains semantically similar classes to those in CIFAR-10, leading to significant overlap between known and unknown categories. This semantic closeness makes unknown detection more challenging, as some unknown samples resemble known classes. However, applying Mixup, label smoothing, and semantic dispersion mitigates this issue by encouraging smoother decision boundaries and reducing overconfidence in ambiguous regions, as illustrated in Fig. 7 and Fig. 8.

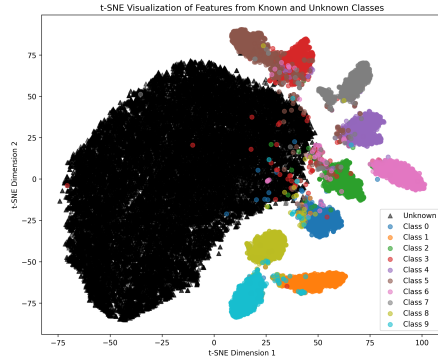


Figure 5. CIFAR-10 as Known, SVHN as Unknown, No Mixup + Label Smoothing.

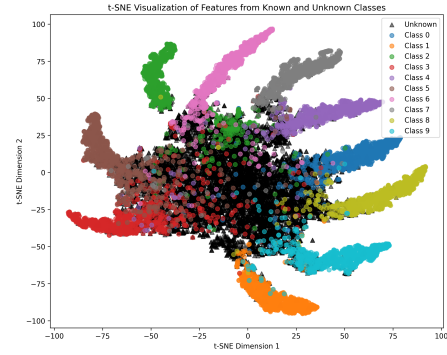


Figure 8. CIFAR-10 as Known, CIFAR-100 as Unknown, With Mixup + Label Smoothing.

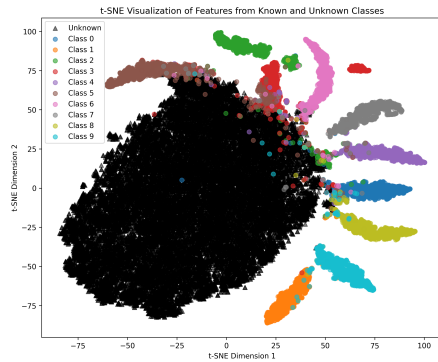


Figure 6. CIFAR-10 as Known, SVHN as Unknown, With Mixup + Label Smoothing.

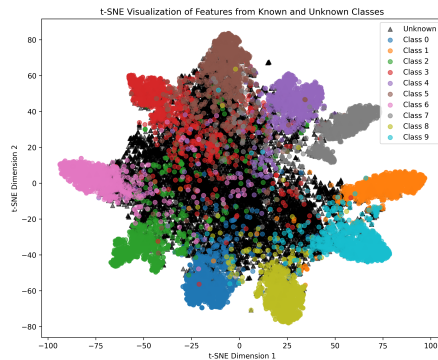
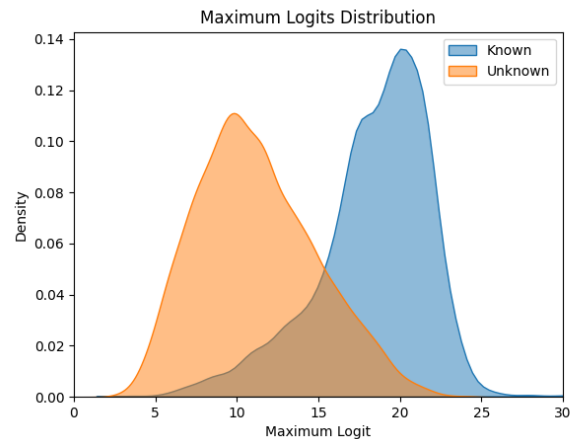


Figure 7. CIFAR-10 as Known, CIFAR-100 as Unknown, No Mixup + Label Smoothing.

### 10.0.2. Logits Distribution Analysis

We also examine the logit distribution across all cases. With label smoothing, from Fig 12 to Fig 11, the logits become more peaked for known classes while flattening for unknowns, indicating that it regulates the feature norm parameters.

We also examine the logit distribution across all cases. With Mixup, as seen from Fig.12 to Fig.9, the peaks of the logits shift in opposite directions, indicating increased separation in the feature space.



(a) Baseline

Figure 9. Distribution of Maximum Logits for CIFAR10 (Known) and CIFAR100 (Unknown) across various training settings with both mixup and no label smoothing

### 10.0.3. GradCAM analysis of SPHOR

SPHOR emphasizes class distinctions by learning highly discriminative features, making them effective for distinguishing known classes but less transferable to novel domains. This property enables classifiers to detect the absence of learned features, which is beneficial for Open-Set

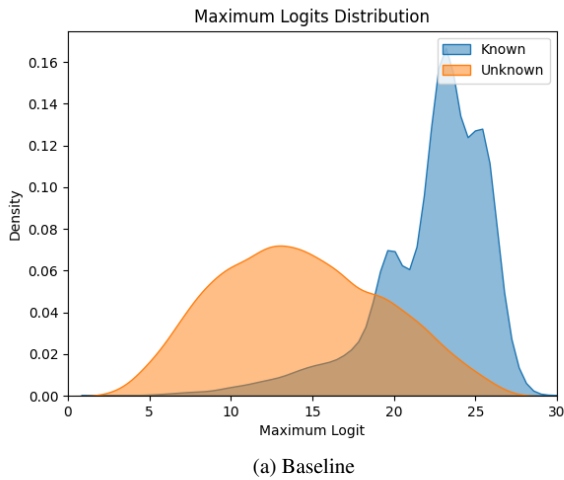


Figure 10. Distribution of Maximum Logits for CIFAR10 (Known) and CIFAR100 (Unknown) across various training settings with both mixup and label smoothing

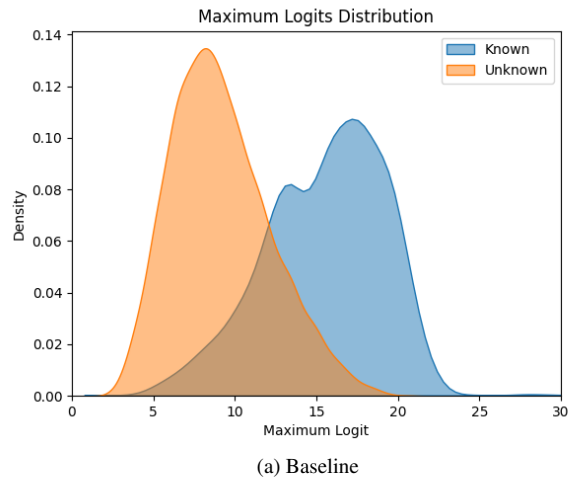


Figure 12. Distribution of Maximum Logits for CIFAR10 (Known) and CIFAR100 (Unknown) across various training settings with no mixup and no label smoothing

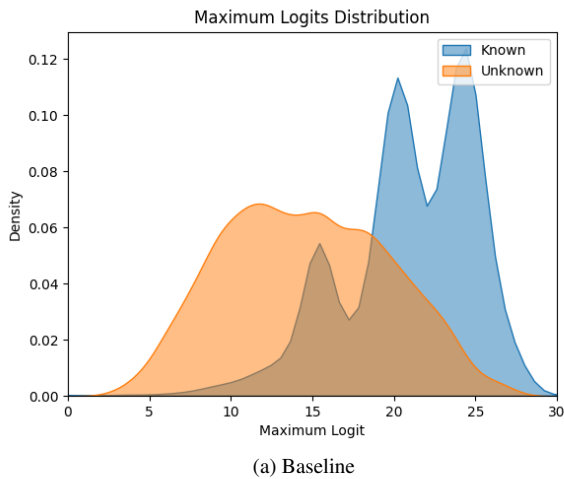


Figure 11. Distribution of Maximum Logits for CIFAR10 (Known) and CIFAR100 (Unknown) across various training settings with both no mixup and with label smoothing

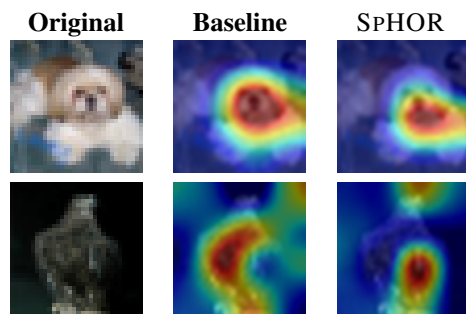


Figure 13. Class activation maps (CAMs) of softmax trained CNN networks and the SPHOR. The images are drawn from and the network is trained on CIFAR10.

Recognition (OSR). Class Activation Maps (CAMs) further highlight differences in feature learning, showing that contrastive learning produces smaller, more concentrated hot zones that focus on discriminative features rather than broadly separable ones.